

Smart Stretchable Janus Membranes with Tunable Collection Rate for Fog Harvesting

Yahui Su, Shengwen Cai, Tao Wu, Chuanzong Li, Zhouchen Huang, Yiyuan Zhang, Hao Wu, Kai Hu, Chao Chen, Jiawen Li, Yanlei Hu, Suwan Zhu,* and Dong Wu*

Water scarcity is one of the severest global resource shortages because freshwater plays a vital role in human existence. Fog harvesting is a promising approach to alleviate freshwater shortage, but most existing strategies based on rigid materials suffer from the shortage of nontunable fog collection rate. Herein, a smart Janus membrane with a tunable fog collection rate via uniaxially stretching a flexible polydimethylsiloxane sheet fabricated by ultrafast laser drilling is reported. Compared to its original form, the maximum strain of 200% shows up to 67% enhancement in its fog collection efficiency. Further theoretical calculation demonstrates that the increase of fog collection rate along with uniaxially stretching is estimated to be $\approx 79\%$ for 200% strain sample based on the cooperation between the wetting driving force and Laplace pressure, which is in well agreement with the experimental result. It is believed that this smart Janus membrane would operate not only in the field of fog harvesting, but also in specific scenarios, such as dynamic fog-flux regulators.

As tiny fog contributes to $\approx 10\%$ component for entire fresh water on the earth, fog harvesting has attracted great attentions due to the shortage of worldwide fresh water resource.^[1–3] Various fog harvesting strategies have been extensively studied via mimicking natural species, such as cactus and Namib desert beetle, etc.^[4–12] For instance, Jiang et al. achieved continuous and efficient fog harvesting by preparing conical copper wires and conical microtips with the cooperation of Laplace pressure and wettability gradients.^[13,14] Wang et al. fabricated a CuO-perfluorodecanethiol-polystyrene (CuO-PFDT-PS) composite surface for fog harvesting by using alternating hydrophobic (HB) and hydrophilic (HL) regions.^[15] Dai et al. realized rapid droplet harvesting and mobility using a bio-inspired slippery rough surface, which had

combined the slippery interface of pitcher plants and the hierarchical micro/nanostructures of rice leaves.^[16] As one of the novel functional materials, Janus membranes (JMs)^[17] with porous structures have been fabricated and employed in the applications including oil/water separation,^[18–20] unidirectional transport of gas bubbles,^[21–23] and fog harvesting.^[24–27] These facile HB/HL JMs showed noteworthy enhancement in fog harvesting compared with previously reported studies.^[25–27] In general, the above-mentioned explorations can be classified into conventional rigid devices, which are limited to their nontunable collection rates.

Recently, smart materials are frequently used in both industrial manufacturing and scientific research due to their abilities of sensing external stimulus from the environment and generating a useful response.^[28–36] As a facile and effective method, stretch strategy is especially suitable for regulating flexible materials, which opens up enormous potential in plentiful applications, such as variable transparency, adaptive adhesion control, droplet manipulator, etc.^[31–36] Specifically, Yao et al. reported a stretchable fluid-infused porous film with tunable transparency and wettability for reversibly controlling the sliding of oil droplets.^[34] Lin et al. fabricated a multiscale self-similar hierarchical wrinkled surface as a multifunctional smart window with simultaneously tunable transparency, structural color, and droplet transport.^[35] Inspired by human skin structures, Wang et al. prepared a smart superhydrophobic (SHB) elastomer polydimethylsiloxane (PDMS) skin with controllable capture and release abilities of water droplet through bending or stretching.^[36] Despite the up-to-date achievements for smart

Prof. Y. Su, S. Cai
School of Electrical Engineering and Automation
Anhui University
Hefei, Anhui 230601, China


Prof. Y. Su
School of Electronics and Information Engineering
Anhui University
Hefei, Anhui 230601, China

Prof. Y. Su
Key Laboratory of Computational Intelligence and Signal Processing
Ministry of Education
Anhui University
Hefei, Anhui 230039, China

T. Wu
Department of Modern Mechanics
University of Science and Technology of China
Hefei, Anhui 230026, China

C. Li
School of Instrument Science and Opto-electronics Engineering
Hefei University of Technology
Hefei, Anhui 230009, China

Z. Huang, Y. Zhang, H. Wu, K. Hu, Dr. C. Chen, Prof. J. Li, Prof. Y. Hu,
Dr. S. Zhu, Prof. D. Wu
CAS Key Laboratory of Mechanical Behavior and Design of Materials
Department of Precision Machinery and Precision Instrumentation
University of Science and Technology of China
Hefei, Anhui 230026, China
E-mail: suwanzhu@ustc.edu.cn; dongwu@ustc.edu.cn

 The ORCID identification number(s) for the author(s) of this article can be found under <https://doi.org/10.1002/admi.201901465>.

DOI: 10.1002/admi.201901465

flexible materials in various functions, it is still lacking relevant studies in the field of fog harvesting with tunable collection performances.

Herein, we report a smart JM with tunable fog collection rate (FCR) via stretching a flexible PDMS sheet fabricated by ultrafast laser drilling^[20,22,23,25] for the first time to our best knowledge. Our experimental results show that FCR can be tuned arbitrarily and reversibly by uniaxially stretching the JM. Compared with its original profile, the maximum strain of 200% shows up to 67% enhancement in FCR. Further calculation demonstrates that the increase of FCR is estimated to be $\approx 79\%$ for 200% strain sample, which is in well agreement with our experimental result. Meanwhile, several consecutive cycles of fog harvesting process show fine collection reproducibility. This study provides a new insight on flexible JMs with a tunable FCR, which would be beneficial for their practical applications not only in fog harvesting, but also in food engineering as dynamic fog-flux regulators, for which regulating initial moisture content and moisture migration is of vital importance for maintaining quality and safety of foods.^[37–39] In other words, one can gain any desirable collection rates through diverse stretching extents.

PDMS is one of the most frequently used materials in both commercial applications and scientific researches owing to its plenty of superiorities including stretchability, excellent oxidation resistance, and easy preparation. The fabrication schematics of our PDMS-based JM are shown in Figure 1a, which can be divided into three steps. First, the homogeneous microhole arrays were manufactured after nanosecond laser microdrilling. The perforating space between two adjacent holes was set as 200 μm . The drilled PDMS membrane was SHB and the water contact angle (WCA) was 154° (Figure S1a, Supporting Information). To better distinguish two sides of the PDMS membrane,

we defined the laser-irradiated surface as the top surface and the other side as the bottom surface. Second, after high surface energy superhydrophilic (SHL) reagent modification, the laser-induced sample was turned into double-faced superhydrophilicity, and both the WCA decreased to 3° (Figure S1b, Supporting Information). Finally, the bottom surface was irradiated through line-by-line femtosecond laser scanning process to remove the previous SHL reagent, resulting in hydrophobic property. On the contrary, laser scanning would not damage the top surface and the inside of the holes, and thus the top surface remained its superhydrophilicity with a WCA of 5° (Figure S1c, Supporting Information). By tuning the force of applied strain on the JM, one can easily realize different fog collection efficiency under variational stretching conditions. Here we define the strain value $\epsilon = (L - L_0)/L_0$, where L and L_0 are the tensile state and the original state, respectively.^[36] The top and bottom optical images of the laser-prepared membrane are shown in Figure 1b,c. From the insets we can obviously observe that the top diameter (120 μm) is greater than the bottom diameter (54 μm). Furthermore, the profile morphology of single conical hole is shown in Figure S2, Supporting Information, from which we can see that various micro- and nanomastoids are produced on the wall of the inner conical hole during laser ablation. The bottom optical images of the Janus membranes with four different strains ($\epsilon = 50\%$, 100%, 150%, and 200%) are shown in Figure 1d–g, and each inset represents the corresponding scanning electron microscope (SEM) image. We define the long axis (along the stretching direction) and short axis (perpendicular to the stretching direction), respectively. For single microhole, it can be seen that the average length of long axis increases with the increase of the strain, but the short axis almost remains unchanged (Figure 1h). The repeated-stretching experiment (in 200% strain, Figure 1i) demonstrates that the average lengths

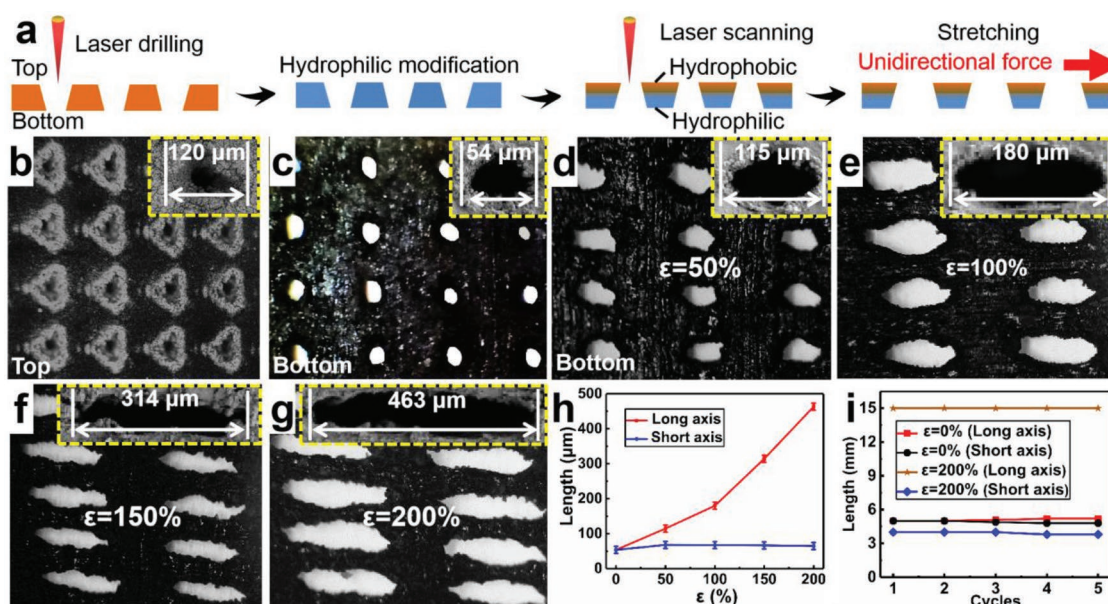


Figure 1. a) Schematic diagrams of JM fabrication and stretching. b,c) Optical images of JM's top and bottom surfaces. d–g) Bottom surfaces of JMs in four different strains ($\epsilon = 50\%$, 100%, 150%, and 200%). The insets of b–g) are SEM images of each magnified microhole. h) Average lengths of long and short axes of single microhole in different strains. i) Average lengths along the long and short axes directions for the processed macroscopic area during five stretching-recovering cycles.

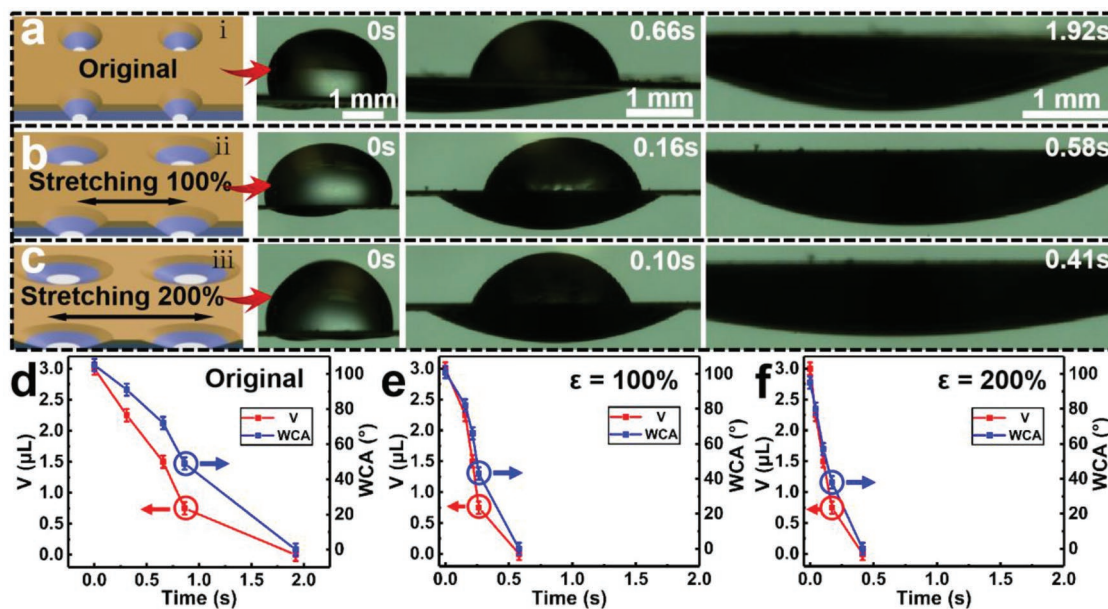


Figure 2. a–c) Stretching schematics of JM for three typical strains ($\epsilon = 0\%$, 100%, and 200%) and corresponding dynamic processes of droplet self-transport. d–f) Volume and WCA changes of the droplets with time on three JM surfaces.

along the long and short axes directions for the processed macroscopic area remain constant during five stretching-recovering cycles, which shows a favorable flexibility for our JM.

To investigate the performance of unidirectional self-transport for water droplet on the JM, samples with three typical strains ($\epsilon = 0\%$, 100%, and 200%) were employed experimentally. Stretching schematics of the PDMS-based JM and dynamic process of the droplet self-transport are shown in Figure 2 and Movie S1, Supporting Information. For original JM, the dynamic WCA of a 3 μL droplet on the bottom surface decreased from 105° to 0° with time, resulting in a complete permeation to the top. Besides, the original membrane showed a maximum WCA (Figure 2d) compared with those of 100% and 200% strain samples (Figure 2e,f) because the surface morphology and shape of the JM played significant roles in regulating WCA.^[31–36] Furthermore, the penetration times of water droplet on the JM were measured as 1.92, 0.58, and 0.41 s, respectively, for the three samples, demonstrating that a 200% strain sample has the fastest droplet penetration capability.

In order to quantify the fog collection efficiency of our JM, a home-made fog harvesting measurement system was employed. As shown in Figure 3a, the measurement system consisted of a timer, a humidifier, and a harvesting device (i.e., a measuring cylinder with a JM fixed tightly on its mouth). The processes of harvesting volume change with time for the harvesting devices in three typical strains ($\epsilon = 0\%$, 100%, and 200%) are shown in Figure 3b–d and Movie S2, Supporting Information. At the initial time of 0 min, 2 mL water dyed with methylene blue was poured into each measuring cylinder. It can be clearly observed that the cylinder with 200% strain sample has the maximum water volume compared with those of the other two cylinders after both 0.5 and 1 h. Specifically, the average collection rates for five different strains ($\epsilon = 0\%$, 50%, 100%, 150%, and 200%) were calculated as 0.031, 0.035,

0.038, 0.047, and 0.052 $\text{mL cm}^{-2} \text{min}^{-1}$ respectively, which were positively related to the strain values, as the blue curve showed in Figure 4a. Meanwhile, we also performed the fog collection for SHL–SHL and SHB–SHB membranes in the same experimental parameters with the JM (Figure S3, Supporting Information). As the red curve shows in Figure S3, Supporting Information, the collection rate of SHB–SHB membrane was close to zero for each strain case, which could be attributed to its high threshold for penetration.^[24–26] For SHL–SHL membrane, the limited increase for FCR was far less than the corresponding increase for that of JM. This reveals that JM has the optimum fog harvesting configuration due to its unique combined action of hierarchical and complementary HB–HL structure from which the water droplet can automatically penetrate the membrane from HB surface to HL surface owing to wetting driving force of the gradient surface face.^[24–27] Besides, the HB and HL surfaces are also beneficial to fog harvesting and water preservation, respectively.

The schematic diagram of fog collection behaviors for JM with different strains ($\epsilon = 0\%$ and 200%) is shown in Figure 4b. The water droplets could rapidly absorb into the HL side due to the cooperation of wetting driving force (F_{wet}) and Laplace pressure ($\Delta F_{\text{Laplace}}$) for JM.^[2,4,12,25,40,41] Once the grown droplets on the HB surface came into contact with the SHL area, it would be simultaneously absorbed and permeated. This rapid permeation process could regenerate a fresh dry surface for droplets easy adhering and condensing, which maintains the continuous process of fog harvesting. It is worth mentioning that water droplets tend to penetrate JM from the boundary between HB and HL areas on the inner conical hole rather than the central area of the hole,^[24,25,27] which explains well the near-zero FCR observed in our SHB–SHB membrane (Figure S3, Supporting Information). Further analysis shows that the FCR of JM has 67% enhancement for the sample in the maximum

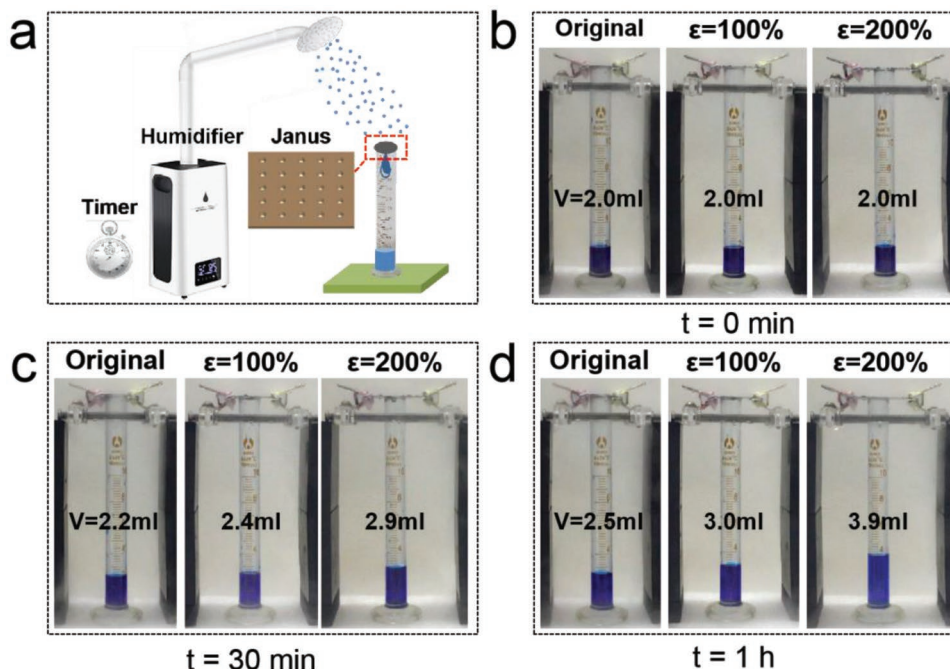


Figure 3. a) Schematic illustration of fog harvesting measurement system. b–d) Snapshots of dynamic collection volumes at $t = 0$ min, 30 min, and 1 h for JMs in three typical strains ($\epsilon = 0\%$, 100% , and 200%).

strain of 200% compared with that of the original membrane. Meanwhile, the porosity of the sample in its maximum strain reached up to 5.2 times the original sample porosity (from 5%

to 26%), as the red curve showed in Figure 4a. In order to clarify the physical mechanism for enhanced FCR in elevated strains, we systematically calculated the dominant forces participating

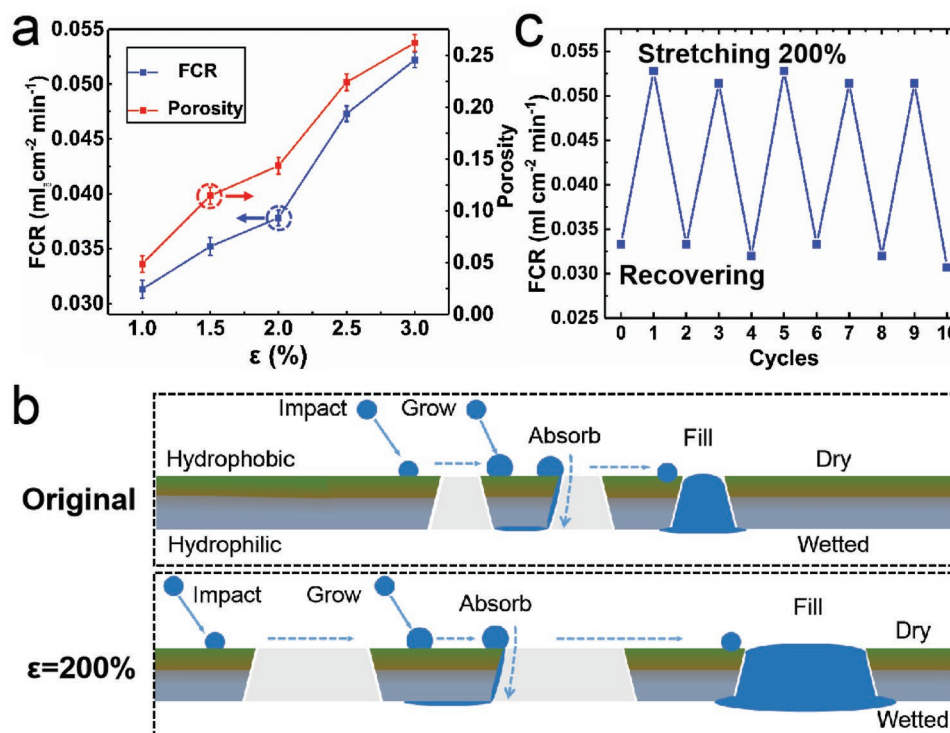


Figure 4. a) Fog collection behaviors of JM with different strains ($\epsilon = 0\%$ and 200%). b) FCR and porosity of JM in different strains ($\epsilon = 0\%$, 50% , 100% , 150% , and 200%). c) FCR of JM under five consecutive stretching-recovering cycles.

in fog harvesting process. The wetting driving force F_{wet} is described as follows^[2,4,25,40]

$$F_{\text{wet}} = \cos \frac{\alpha}{2} \int_{\theta_{\text{bottom}}}^{\theta_{\text{top}}} -L \times \gamma \times \sin \theta \, d\theta \quad (1)$$

where α , γ , L , θ_{bottom} , and θ_{top} are the tip angle of conical micropore, water surface tension ($7.2 \times 10^{-2} \text{ N m}^{-1}$), the micropore perimeter for bottom side and the WCAs on the bottom and top of conical micropores, respectively. For the samples of $\varepsilon = 0\%$ and $\varepsilon = 200\%$, the values of θ_{bottom} versus θ_{top} were estimated to be 105° versus 5° and 95° versus 5° , respectively. Hence, F_{wet} were roughly estimated to be 1.46×10^{-5} and $7.69 \times 10^{-5} \text{ N}$ for the two samples when the conical micropore was filled with water. The Laplace pressure is described as follows^[2,4,12,41]

$$\Delta F_{\text{Laplace}} = \Delta S \times \gamma \times \left(\frac{1}{R_1} + \frac{1}{R_2} \right) \quad (2)$$

where ΔS , R_1 , and R_2 are the micropore area for bottom side, radii of curvature for arbitrary two orthogonal directions on the droplet surface in the bottom area of the inner conical pore. Specifically, ΔS could be regarded as a circle with radius of $\approx 2.7 \times 10^{-5} \text{ m}$ for $\varepsilon = 0\%$ sample, and R_1 (equal to R_2) was estimated to be $\approx 4.86 \times 10^{-5} \text{ m}$. In contrast, for the stretched sample in $\varepsilon = 200\%$ strain, ΔS was approximate to an ellipse with long and short axes of $\approx 2.3 \times 10^{-4}$ and $\approx 3.0 \times 10^{-5} \text{ m}$, respectively. In this case, R_1 and R_2 were estimated to be $\approx 4.5 \times 10^{-3}$ and $\approx 1.1 \times 10^{-4} \text{ m}$, respectively. As a result, $\Delta F_{\text{Laplace}}$ were calculated as $\approx 6.78 \times 10^{-6}$ and $\approx 1.52 \times 10^{-5} \text{ N}$, respectively, and the self-driving force $F_{\text{self-drive}}$ (equal to $F_{\text{wet}} + \Delta F_{\text{Laplace}}$) were obtained near $\approx 2.14 \times 10^{-5}$ and $\approx 9.21 \times 10^{-5} \text{ N}$, respectively, for the two samples. To compare the FCR differences for the two samples, the calculated $F_{\text{self-drive}}$ should be divided by the increased ratio of ≈ 2.4 that stems from the stretched laser-processed area. The theoretical increase rate of $\approx 179\%$ is slightly larger than the experimental result of 167% in FCR, which is probably due to the rational deviation in our mechanical model. Finally, stretch limit and repeatability are also crucial parameters for evaluating smart flexible materials. The stretch limit was evaluated through a tensiometer in different strains and schematically shown in Figure S4 and Movie S3 (Supporting Information). Experimental results show that when an external force that imposes on the JM exceeds 4.6 N ($\approx 250\%$ in its strain), the membrane would break. Accordingly, the fog harvesting repeatability was also evaluated for the JM under consecutive stretching-recovering cycles. Figure 4c shows five representative cyclic for our JM device. Notably, the device shows a similar collection rate in each stretching-recovering cycle, which suggests its favorable repeatability. It is worth noting that mechanical fatigue was not the main factor that accounts for function failure in our Janus membrane without exceeding the stretch limit (Figure S4, Supporting Information). Essentially, the durability is determined by SHL reagent due to the consumption (i.e., mass loss) during fog collection process, in which water may take the reagent away through dissolution. The dissolution speed for different SHL product may vary distinctly. For the SHL agent employed in this paper (MesoBioSys. Co., Ltd., Wuhan, China), our Janus device could function well up to 10 cycles, whereas the exact lifetime might vary in each independent case. Though the

moderate stability of this SHL agent hinders this Janus membrane toward its practical applications, we convince that people would solve this engineering issue with the fast development of commercial SHL solvents inspired by the current work. For emphasis, our current work is focusing on the demonstration for the proof-of-concept regulating FCR by utilizing this dynamically responsive Janus membrane, which provides a widely adaptive approach for people fabricating smart devices in terms of fog harvester, and further bloom the researchers in micro/nano fabrications, microfluidics, and fog-involved regulators.

In summary, we put forward a smart JM for fog harvesting using a flexible PDMS sheet fabricated through ultrafast laser drilling and subsequent selective surface modification. Different from traditional rigid fog collection devices that suffer from the shortage of nontunable collection rate, our flexible JM shows a tunable FCR via uniaxially stretching method. Compared with original JM, the maximum strain of 200% in length shows up to 67% enhancement in its FCR. Further study demonstrates that the theoretical increase of FCR is estimated to be $\approx 79\%$ for 200% strain sample, which is in well agreement with our experimental result. It is worth mentioning that the morphology and performance of the smart JM can be easily tuned using other flexible materials under different laser-ablating conditions, which means that one can get any desirable collection rates for different applications through stretching strategy. We believe that this smart JM would operate not only in the field of fog harvesting, but also in other specific scenarios such as dynamic fog-flux regulators in food engineering, for which moisture control within a certain range is crucial for producing safe products with optimum shelf-life.

Experimental Section

Materials: The average thickness of the black commercially available PDMS sheets were $\approx 100 \mu\text{m}$ for laser processing, and were purchased from Hangzhou BALD Advanced Materials Tech. Co., Ltd., Hangzhou, China. The SHL reagent (MesoBioSys. Co., Ltd., Wuhan, China) were used to increase the surface energy of samples. The distilled water (H_2O , 1 g cm^{-3} density) and NPT (normal pressure and temperature) air (20°C , 1 atm , $1.205 \times 10^{-3} \text{ g cm}^{-3}$ density) were served as test material in the contact angle and fog harvesting measurement.

Microstructure Fabrication: The microhole-arrayed SHB membranes were prepared by repeatedly drilling through a nanosecond laser, and the processing area was $5 \times 5 \text{ mm}$. The laser beam (10 ns , 10 Hz , 355 nm) from a neodymium doped yttrium aluminum garnet nanosecond laser system (Spectra-Physics) was employed for ablation. The SHB membranes were initially modified by the SHL reagent and then ablated to remove the SHL reagent for the bottom surface using a line-by-line femtosecond laser scanning process, resulting in the JM. The laser beam (400 fs) with a repetition rate of 1 MHz at a central wavelength of 1030 nm was supplied by a commercial high repetition femtosecond laser system (Menlosystems). The laser power, scanning spacing, and scanning speed were 100 mW , $20 \mu\text{m}$, and 100 mm s^{-1} .

Instruments and Characterizations: The WCAs were measured by using a contact angle system (CA100D, Innuo, China) with $5 \mu\text{L}$ water droplets on the as-prepared samples at different locations under 10% relative humidity and 20°C temperature, respectively. Surface micro- and nanostructures of the JM were characterized by a secondary scanning electron microscope (Zeiss EVO18, Germany) with an accelerating voltage at 10 keV . The dynamic process that the water droplet ($3 \mu\text{L}$) penetrated through the JM was recorded using a high-speed video camera (Photron Fastcam SA6, USA) at a typical rate of 500 fps .

Tunable Fog Harvesting Strategy: The as-prepared sample membranes with a hole distance of 200 μm were fixed at 6 cm below the nozzle of a home-made measurement system in which simulated fog was generated with a flow velocity of about 70 cm s^{-1} . For comparing collection efficiency of the membranes, three PDMS samples with different wettability gradients including HB-SHL (JM), SHB-SHB, and SHL-SHL membranes were fabricated. For each membrane, five independent experiments in different strains ($\epsilon = 0\%$, 50%, 100%, 150%, and 200%) were operated for fog harvesting, and 2 mL water dyed with methylene blue was poured into each measuring cylinder beforehand. Finally, the consecutive cycling experiments between strains of $\epsilon = 0\%$ and 200% were performed to investigate the fog collection reproducibility.

Supporting Information

Supporting Information is available from the Wiley Online Library or from the author.

Acknowledgements

This work was supported by Key Project of Equipment Pre-research Field Fund in China (No. 61409230310), Anhui Provincial Natural Science Foundation (No. KJ2018A0014), Foundation of Equipment Development Department (No. 6220914010901), Thousand Young Talents Program of China, National Natural Science Foundation of China (Nos. 11772327 and 11621202), Fundamental Research Funds for the Central Universities (Nos. WK2090050041 and WK2090090024) and China Postdoctoral Science Foundation (No. BH2090000025).

Conflict of Interest

The authors declare no conflict of interest.

Keywords

fog harvesting, Janus membranes, smart materials, tunable collection rate, ultrafast laser fabrication

Received: August 23, 2019
Revised: September 11, 2019
Published online:

- [1] S. Zhang, J. Huang, Z. Chen, Y. Lai, *Small* **2017**, *13*, 1602992.
[2] H. Zhu, Z. Guo, W. Liu, *Chem. Commun.* **2016**, *52*, 3863.
[3] J. Ju, Y. Zheng, L. Jiang, *Acc. Chem. Res.* **2014**, *47*, 2342.
[4] J. Ju, H. Bai, Y. Zheng, T. Zhao, R. Fang, L. Jiang, *Nat. Commun.* **2012**, *3*, 1247.
[5] H. Bai, C. Zhang, Z. Long, H. Geng, T. Ba, Y. Fan, C. Yu, K. Li, M. Cao, L. Jiang, *J. Mater. Chem. A* **2018**, *6*, 20966.
[6] A. R. Parker, C. R. Lawrence, *Nature* **2001**, *414*, 33.
[7] H. Zhu, Z. Guo, *Chem. Commun.* **2016**, *52*, 6809.
[8] K. Yin, H. Du, X. Dong, C. Wang, J.-A. Duan, J. He, *Nanoscale* **2017**, *9*, 14620.
[9] H. Bai, L. Wang, J. Ju, R. Sun, Y. Zheng, L. Jiang, *Adv. Mater.* **2014**, *26*, 5025.
[10] H. Bai, J. Ju, Y. Zheng, L. Jiang, *Adv. Mater.* **2012**, *24*, 2786.
[11] Y. Zheng, H. Bai, Z. Huang, X. Tian, F.-Q. Nie, Y. Zhao, J. Zhai, L. Jiang, *Nature* **2010**, *463*, 640.
[12] X. Ma, M. Cao, C. Teng, H. Li, J. Xiao, K. Liu, L. Jiang, *J. Mater. Chem. A* **2015**, *3*, 15540.
[13] J. Ju, K. Xiao, X. Yao, H. Bai, L. Jiang, *Adv. Mater.* **2013**, *25*, 5937.
[14] M. Cao, J. Ju, K. Li, S. Dou, K. Liu, L. Jiang, *Adv. Funct. Mater.* **2014**, *24*, 3235.
[15] Y. Wang, L. Zhang, J. Wu, M. N. Hedhili, P. Wang, *J. Mater. Chem. A* **2015**, *3*, 18963.
[16] X. Dai, N. Sun, S. O. Nielsen, B. B. Stogin, J. Wang, S. Yang, T.-S. Wong, *Sci. Adv.* **2018**, *4*, eaag0919.
[17] H. Yang, Y. Xie, J. Hou, A. K. Cheetham, V. Chen, S. B. Darling, *Adv. Mater.* **2018**, *30*, 1801495.
[18] X. Tian, H. Jin, J. Sainio, R. H. A. Ras, O. Lkkala, *Adv. Funct. Mater.* **2014**, *24*, 6023.
[19] Y.-P. An, J. Yang, H.-C. Yang, M.-B. Wu, Z.-K. Xu, *ACS Appl. Mater. Interfaces* **2018**, *10*, 9832.
[20] J. Yong, Q. Yang, C. Guo, F. Chen, X. Hou, *RSC Adv.* **2019**, *9*, 12470.
[21] R. Waldman, H. Yang, D. J. Mandia, P. F. Nealey, J. W. Elam, S. B. Darling, *Adv. Mater. Interfaces* **2018**, *5*, 1800658.
[22] S. Yan, F. Ren, C. Li, Y. Jiao, C. Wang, S. Wu, S. Wei, Y. Hu, J. Li, Y. Xiao, Y. Su, D. Wu, *Appl. Phys. Lett.* **2018**, *113*, 261602.
[23] C. Chen, L.-A. Shi, Z. Huang, Y. Hu, S. Wu, J. Li, D. Wu, J. Chu, *Adv. Mater. Interfaces* **2019**, *6*, 1900297.
[24] M. Cao, J. Xiao, C. Yu, K. Li, L. Jiang, *Small* **2015**, *11*, 4379.
[25] F. Ren, G. Li, Z. Zhang, X. Zhang, H. Fan, C. Zhou, Y. Wang, Y. Zhang, C. Wang, K. Mu, Y. Su, D. Wu, *J. Mater. Chem. A* **2017**, *5*, 18403.
[26] K. Yin, S. Yang, X. Dong, D. Chu, J.-A. Duan, J. He, *ACS Appl. Mater. Interfaces* **2018**, *10*, 31433.
[27] R. Hu, N. Wang, L. Hou, Z. Cui, J. Liu, D. Li, Q. Li, H. Zhang, Y. Zhao, *J. Mater. Chem. A* **2019**, *7*, 124.
[28] W. Sun, S. Zhou, B. You, L. Wu, *J. Mater. Chem. A* **2013**, *1*, 3146.
[29] D. Zhao, R. Jia, N. Gao, W. Yan, L. Zhang, X. Li, D. Liu, *J. Phys. Chem. C* **2017**, *121*, 12745.
[30] J. Yong, F. Chen, Q. Yang, Y. Fang, J. Huo, X. Hou, *Chem. Commun.* **2015**, *51*, 9813.
[31] Y. Wang, B. Qian, C. Lai, X. Wang, K. Ma, Y. Guo, X. Zhu, B. Fei, J. H. Xin, *ACS Appl. Mater. Interfaces* **2017**, *9*, 24428.
[32] M. Coux, C. Clanet, D. Quéré, *Appl. Phys. Lett.* **2017**, *110*, 251605.
[33] M. Liu, F. Liu, X. Xu, D. Yu, I. Wyman, H. Yang, J. Wang, X. Wu, *ACS Appl. Mater. Interfaces* **2019**, *11*, 16914.
[34] X. Yao, Y. Hu, A. Grinthal, T.-S. Wong, L. Mahadevan, J. Aizenberg, *Nat. Mater.* **2013**, *12*, 529.
[35] G. Lin, P. Chandrasekaran, C. Lv, Q. Zhang, Y. Tang, L. Han, J. Yin, *ACS Appl. Mater. Interfaces* **2017**, *9*, 26510.
[36] J.-N. Wang, Y.-Q. Liu, Y.-L. Zhang, J. Feng, H. Wang, Y.-H. Yu, H.-B. Sun, *Adv. Funct. Mater.* **2018**, *28*, 1800625.
[37] M. A. Reinheimer, S. Mussati, N. J. Scenna, *J. Food Eng.* **2010**, *101*, 409.
[38] T. P. Labuza, C. R. Hyman, *Trends Food Sci. Technol.* **1998**, *9*, 47.
[39] V. V. Lisovsky, *Meas. Sci. Technol.* **2007**, *18*, 1016.
[40] M. Zhang, L. Wang, Y. Hou, W. Shi, S. Feng, Y. Zheng, *Adv. Mater.* **2015**, *27*, 5057.
[41] M. Prakash, D. Quéré, J. W. M. Bush, *Science* **2008**, *320*, 931.